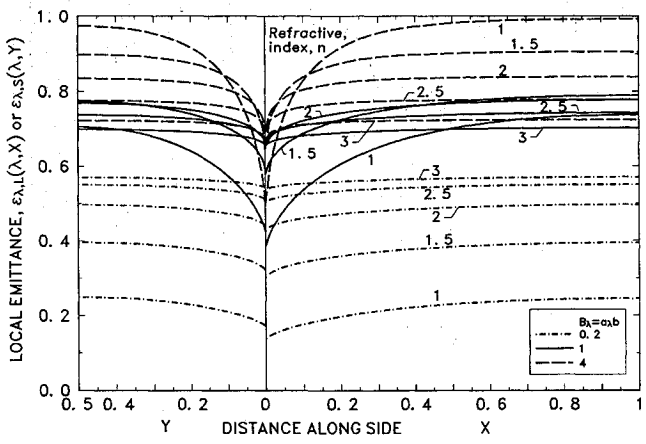

Fig. 2 Local emittances from the sides of a two-dimensional solid with a rectangular cross section of aspect ratio 2, as a function of its refractive index and the optical thickness of the short side.

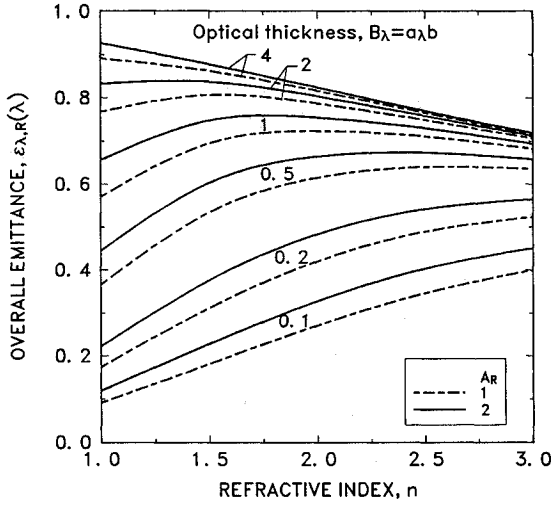

Fig. 3 Integrated average emittance from a two-dimensional rectangular solid with aspect ratios 1 and 2 as a function of its refractive index and the optical thickness of the short side.

they increase for n up to about 2.5; they then decrease as n becomes larger. At the center of the side, ε_λ decreases with increasing n. As n is increased, the emittance becomes more uniform across the side.

Figure 2 gives local ε_λ along the short and long sides of a rectangle with $A_R = 2$. The $\varepsilon_L(X)$ and $\varepsilon_S(Y)$ behavior with n and $a_\lambda b$ is similar to Fig. 1. At the corner there is a small difference in the local emittances on the two sides. This difference is very small when either n or $a_\lambda b$ is large. For large $a_\lambda b$ the behavior in the corner region becomes radiatively isolated from the other parts of the volume; the $\varepsilon_L(X)$ and $\varepsilon_S(Y)$ variations along the two sides tend to become the same in the corner region.

The integrated average emittances are in Fig. 3 as a function of refractive index for $A_R = 1$ and 2; these can be used to compute the overall heat loss for any T_M and T_E, and for a spectral variation of a_λ. The trends are in accord with those in Figs. 1 and 2. For small $a_\lambda b$, the overall spectral emittance $\varepsilon_{\lambda,R}(\lambda)$ increases as n is increased. For a large $a_\lambda b$ this trend is reversed. For intermediate $a_\lambda b$, the overall emittance passes through a maximum with increasing n.

Conclusions

Local and integrated average spectral emittances are obtained around the boundary of a two-dimensional rectangular solid at uniform temperature and with a refractive index larger than one. Radiation at the boundaries is assumed diffuse, and internal reflections are included. The results show the effect on emittance of refractive index, optical thickness $a_\lambda b$, and aspect ratio. For an optically thin region with $a_\lambda b$ less than about 1, the local and overall emission increase as refractive index increases. For $a_\lambda b$ larger than about 2.5 the trend is reversed, and so increasing n results in decreased emission. The minimum local emittance occurs at the corners. An increased refractive index causes the local emittance to be more uniform over each side of the rectangle.

References

[1]Wu, C. Y., Sutton, W. H., and Love, T. J., "Directional Emittance of a Two-Dimensional Scattering Medium with Fresnel Boundaries," *Journal of Thermophysics and Heat Transfer*, Vol. 3, No. 3, 1989, pp. 274–282.

[2]Siegel, R., "Analytical Solution for Boundary Heat Fluxes from a Radiating Rectangular Medium," *Journal of Heat Transfer*, Vol. 113, No. 1, 1991, pp. 258–261.

[3]Siegel, R., "Relations for Local Radiative Heat Transfer Between Rectangular Boundaries of an Absorbing-Emitting Medium," *Journal of Heat Transfer*, Vol. 115, No. 1, 1993, pp. 272–276.

[4]Yuen, W. W., and Wong, L. W., "Numerical Computation of an Important Integral Function in Two-Dimensional Radiative Transfer," *Journal of Quantitative Spectroscopy and Radiative Transfer*, Vol. 29, No. 2, 1983, pp. 145–149.

[5]Siegel, R., and Howell, J. R., *Thermal Radiation Heat Transfer*, 3rd ed., Hemisphere, Washington, DC, 1992.

[6]Siegel, R., "Boundary Heat Fluxes for Spectral Radiation from a Uniform Temperature Rectangular Medium," *Journal of Thermophysics and Heat Transfer*, Vol. 6, No. 3, 1992, pp. 543–545.

Surface Radiation for Rectangular Enclosures Using the Discrete-Ordinates Method

J. R. Ehlert* and T. F. Smith†
University of Iowa, Iowa City, Iowa 52242

Introduction

SÁNCHEZ and Smith[1] formulated the discrete-ordinates method (DOM) for radiant exchange between surfaces separated by a transparent medium for a two-dimensional geometry and demonstrated that the DOM predicted accurate heat fluxes when compared to those of the radiosity/irradiation method (RIM). The purpose of this study is to apply the DOM to compute the radiant exchange for a three-dimensional rectangular enclosure. The formulation is based on that provided by Sánchez and Smith.

Analysis

The rectangular enclosure has lengths of $L_{x,y,z}$ for the x, y, and z axes. The enclosure may contain protrusions and obstructions. The enclosure surfaces, protrusions, and obstructions are diffusely emitting and reflecting, are radiatively opaque, and may have nonuniform radiative property and temperature distributions. The radiative properties are independent of temperature, although this may be relaxed. Openings in the enclosure walls, if present, are represented

Received Aug. 12, 1993; revision received Dec. 3, 1993; accepted for publication Dec. 3, 1993.

*Research Assistant, Department of Mechanical Engineering.
†Professor, Department of Mechanical Engineering. Senior Member AIAA.

by pseudoblack, isothermal surfaces. The intervening medium is radiatively transparent, and polarization effects are neglected.

The spatial and directional discretization of the radiative transfer equation is obtained by dividing the solution domain into control volumes of number $N_{x,y,z}$ for the x, y, and z axes. A general control volume P of dimensions $\Delta x(=L_x/N_x)$, $\Delta y(=L_y/N_y)$, and $\Delta z(=L_z/N_z)$ is surrounded by control volumes (east) E, (south) S, (west) W, (north) N, (front) F, and (back) B. The interfaces between control volume P and the surrounding control volumes are designated by e, s, w, n, f, and b. The directions of propagation of the radiant intensity are discretized with the intensity for control volume P in the discrete direction i designated as I_i^P. For the positive x, y, and z axes, and for the ith direction, intensities entering and leaving control volume P are I_i^{wr}, I_i^{sr}, I_i^{br}, and I_i^e, I_i^n, I_i^f. Corresponding intensities for the negative x, y, and z axes can be defined. The intensity at point P is given as[2]

$$I_i^P = \frac{\mu_i I_i^{wr}/\Delta x + \eta_i I_i^{sr}/\Delta y + \zeta_i I_i^{br}/\Delta z + \alpha\kappa_P I_b^P}{\mu_i/\Delta x + \eta_i/\Delta y + \zeta_i/\Delta z + \alpha\kappa_P} \quad (1)$$

μ_i, η_i, and ζ_i are positive direction cosines from the x, y, and z axes for the ith direction, where $i = 1$ to M, with M denoting the number of discrete directions per octant. α is the finite difference weighting factor. The absorption coefficient κ_P is 0 m^{-1} for a transparent control volume and is assigned a very large value (e.g., 10^{20} m^{-1}) for a solid control volume. The values of κ_P can be keyed to the value of the viscosity that is assigned a large value to represent solid regions.[3] Relations describing the intensities entering and leaving a control volume and a description of interfacial radiative properties are given by Sánchez and Smith.[2]

After experimenting with several quadrature sets,[4-6] a quadrature set based on equal weights and satisfying odd moments (EWO) was chosen. Heat fluxes computed using EWO are found to be more accurate than those using other quadrature sets. The value of α is varied to find the optimum value that yields the minimum error in heat fluxes between the DOM and RIM or Monte Carlo method (MCM). The solution procedure for the radiant intensities and the checking of the overall energy balance are similar to those used by Sánchez and Smith.[1]

Heat fluxes for the DOM are compared to those obtained from the RIM[7] using the view factor expressions for parallel and perpendicular rectangular plates[8] and from the Monte Carlo method (MCM).[9] Because of the difficulty of obtaining view factors for three-dimensional geometries, the comparisons to the RIM are limited to geometries with no protrusions or obstructions. To maintain accuracy in the MCM, the number of rays for each surface element used to compute the view factors is 10,000. Because of the finite number of rays, the view factors do not satisfy the enclosure relation and, therefore, are renormalized so that they sum to unity.

Results and Discussion

The accuracy of the DOM is examined using two test samples: 1) a rectangular enclosure with no protrusions and obstructions, and 2) a rectangular enclosure with a centered obstruction. One goal of the comparisons is to establish values of α, M, and the grid spacing that yield accurate radiant fluxes. For the RIM and MCM, the walls of the enclosure are divided like those for the DOM. The obstruction surfaces are divided into elemental areas equal to those of the opposite enclosure walls.

Empty Enclosure

For sample 1, a cubic enclosure with $L_{x,y,z} = 1.0$ m is considered. One wall of the enclosure has an isothermal temperature of 400 K, and the other walls are at 300 K. All surfaces are black. As noted by Sánchez and Smith, maximum errors are found when the surfaces are black. α is varied from 0.5 to 1.0, N is set at 4, 6, 8, 10, where $M = N(N + 2)/N$, and $N_{x,y,z}$ are varied from 6 to 18. The maximum values for $N_{x,y,z}$ and N are limited by the available memory on the computer system on which the computations were performed. To identify the error between local heat fluxes computed using the RIM and DOM, the root-mean-square (rms) error is used.[1]

Figure 1 shows the rms error as a function of α for $N = 4$, 6, 8, and 10, and $N_{x,y,z} = 10$. The results for $N = 4$ have a maximum rms error of about 0.5 at $\alpha = 0.5$, and decrease to a minimum error of about 0.23 at $\alpha = 1.0$. Results for $N = 6$, 8, and 10 have a maximum rms error at $\alpha = 0.5$, but have a minimum error prior to $\alpha = 1.0$, where the errors are near 0.1. A value of $N = 10$ produces the smallest rms error of about 4% at $\alpha = 0.7$. As N is increased, the rms error minimum occurs at smaller values of α. The difference between the minimum rms error for the different values of N decreases as N is increased. Thus, the minimum rms error for $N = 8$ is close to that of the minimum rms error for $N = 10$, even though the results for $N = 8$ are computed using 40 fewer directions. This finding is important because the additional directions require extra computational time. For example, the case for $N = 8$ takes 12.6 central processing unit seconds (cpus) vs 18.9 cpus for $N = 10$ on a computer system with four 7.5 Mflop central processing units and 64 MB RAM.

Results for the rms error as a function of α are shown in Fig. 2 for $N = 10$ and $N_{x,y,z}$, ranging from 6 to 18. The rms error for the 12 × 12 × 12 grid is larger than that for the 18 × 18 × 18 grid at $\alpha = 0.5$. Increasing the number of control volumes flattens out the slope of the curve for the rms error. For $\alpha = 1$, the rms error decreases as the number of grid points increases. An optimum value of α is found for each grid spacing. For the cases in Fig. 2, the lowest error is found for the 6 × 6 × 6 grid with $\alpha = 0.6$.

The optimum values of α for each nodal value for $N = 8$ and 10 are shown in Fig. 3 as a function of the grid spacing. A value of $\Delta\alpha = 0.01$ is used to identify the optimum value of α. The curves for $N = 8$ and 10 display the same general trend of being nearly linear and sloping upward as the number of nodes increases. Figure 3 shows that, as the number of

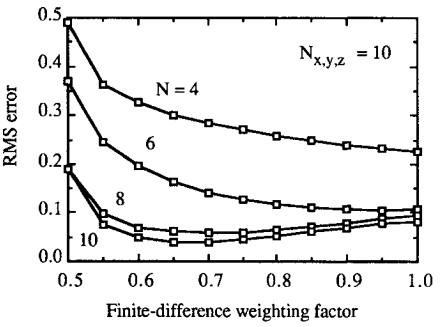

Fig. 1 Root-mean-square error vs finite difference weighting factor (DOM vs RIM).

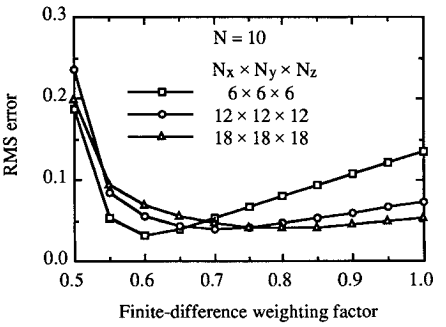

Fig. 2 Effect of number of grid points on rms error (DOM vs RIM).

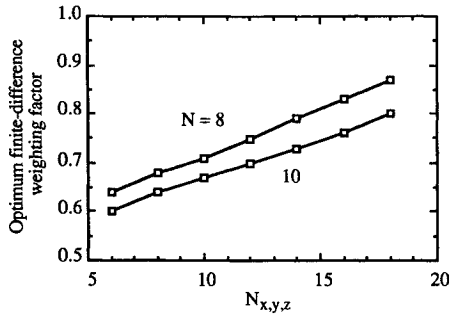

Fig. 3 Effect of the number of control volumes on optimum value of α (DOM vs RIM).

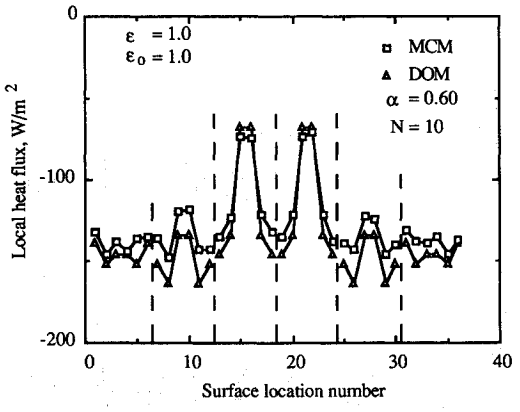

Fig. 4 Local heat fluxes for east wall for case 1 (DOM vs MCM).

control volumes increases, the optimum value of α approaches unity.

Another test case is studied to examine whether changing the shape of the enclosure affects the findings in Fig. 3. The test case is a black wall enclosure with $L_{x,y,z}$ = 0.5, 0.8, 0.9 m. The optimum value of α is found for N = 10 and $N_{x,y,z}$ = 6–18. The curve for this case is shifted upwards by approximately α = 0.02 from the curve for N = 8 in Fig. 3. Thus, the geometry of the problem affects the optimum value of α.

Centered Obstruction

Sample 2 involves a square enclosure with a square, centered obstruction. The MCM is used for comparisons. A small difference in the results for the DOM and MCM is attributed to the MCM using σ = 5.676 × 10^{-8} W/m^2-K^4, rather than σ = 5.669 × 10^{-8} W/m^2-K^4 used by the DOM, a difference of 0.1%. The enclosure has $L_{x,y,z}$ = 0.12 m and $N_{x,y,z}$ = 6. The obstruction has $L_{0x,0y,0z}$ = 0.04 m and $N_{0x,0y,0z}$ = 2. The MCM required on the order of 10 h of cpu time to compute the view factors and heat fluxes on a workstation comparable to that used for the DOM,[9] whereas the DOM took about 2–3 min of cpu time.

Five cases are examined. For case 1, one wall of the enclosure is at 400 K and views an isothermal enclosure at 300 K. For case 2, the enclosure walls are set to 300 K and the walls of the obstruction are set to 400 K. For cases 3–5, two opposite walls of the enclosure are at 400 K while the other walls of the enclosure and the obstruction are set to 300 K. The enclosure surfaces are black for cases 1–3, and have an emittance of 0.5 for cases 4 and 5. The obstruction surfaces are black for cases 1–4 and have an emittance (ε_0) of 0.5 for case 5. α is varied between 0.5–1.0 in increments of 0.05 to find the optimum value that yields the minimum rms error, and N = 10 for the DOM.

The rms errors are approximately 6% for cases 1 and 2, 3% for case 3, and 1% for cases 4 and 5. The optimum values of α vary from 0.60 to 0.65. The optimum value of α from Fig. 3 is 0.6 for $N_{x,y,z}$ = 6. Thus, the results for the obstruction cases are similar to those of the empty enclosure case.

The ability of the DOM to predict local heat fluxes is examined for case 1 in Fig. 4. The surface location numbers for the heat fluxes for the wall of the enclosure opposite the wall at 400 K (called the east wall) are numbered from the origin side corner down along the z axis until the end of the wall is reached. The numbering continues on the next row and follows the form of the bottom row until the top of the wall is reached. The figure has dashed lines to represent the separation between rows. A comparison is made between the heat fluxes of the east wall for the DOM and MCM. This wall has shadowing effects caused by the centered obstruction. For the stated arrangement of temperatures, the heat flux is zero at the exact center of the east wall. Because of the finite size of the surfaces, the DOM and MCM give average heat fluxes for each surface. Surface location numbers 15, 16, 21, and 22 show this as these heat fluxes are smaller (small absolute value) than those for the rest of the wall. The heat fluxes for surface locations 1–14, 17–20, and 23–36 are high (large absolute value) because these surfaces directly view the high-temperature west wall. The DOM slightly overpredicts the MCM heat fluxes except for the shadowed area. The heat flux values for the DOM and MCM are closer for the shadowed areas than for the unshadowed areas. The geometry of the case dictates the solution to be symmetric. The DOM heat fluxes are symmetric, but the MCM heat fluxes exhibit some distortion. Overall, there is good agreement between the local heat fluxes for the DOM and MCM.

Conclusions

A three-dimensional model based on the discrete-ordinates method has been developed for the evaluation of radiant exchange between surfaces separated by a transparent medium. Validation of the model was accomplished by comparing local heat fluxes to those computed from the radiosity/irradiation method and the Monte Carlo method. The comparisons revealed that the heat fluxes from the model are in good agreement with those from the other methods. For the cases considered, a value of α between 0.6–0.8 yields accurate results using N = 10.

Acknowledgments

The authors wish to acknowledge support for this study by the Rockwell International Corporation. The authors thank W. D. Fischer of The Aerospace Corporation for providing the radiant heat flux results from the Monte Carlo method.

References

[1]Sánchez, A., and Smith, T. F., "Surface Radiation Exchange for Two-Dimensional Rectangular Enclosures Using the Discrete-Ordinates Method," *Journal of Heat Transfer*, Vol. 114, No. 2, 1992, pp. 465–472.

[2]Haferman, J. L., Krajewski, W. F., Smith, T. F., and Sánchez, A., "Radiative Transfer for a Three-Dimensional Rainy Cloud," *Applied Optics*, Vol. 32, No. 15, 1993, pp. 2795–2802.

[3]Smith, T. F., Beckermann, C., and Adams, C. C., "A Numerical Simulation Model to Study Window Thermal Performance," American Society of Heating, Refrigerating and Air-Conditioning Engineers, ASHRAE Paper DE-93-4-4, 1993.

[4]Fiveland, W. A., "The Selection of Discrete Ordinate Quadrature Sets for Anisotropic Scattering," *Fundamentals of Radiation Heat Transfer*, American Society of Mechanical Engineers HTD-Vol. 160, 1991, pp. 89–96.

[5]Thurgood, C. P., Becker, H. A., Grandmaison, E. W., Pollard, A., Rubini, P., and Sobiesiak, A., "Development of T_N Quadrature Sets and HEART Solution Method for Calculating Radiative Heat Transfer," *Experimental Heat Transfer, Fluid Mechanics, and Thermodynamics, Proceedings of the 2nd World Conference* (Dubrovnik, Yugoslavia), edited by J. F. Keffer et al., Elsevier, 1991, pp. 613–620.

[6]Sacadura, J. F., and El Wakil, N., "Some Improvements of the Discrete Ordinates Method for the Solution of the Radiative Trans-

port Equation in Multidimensional Anisotropically Scattering Media," *Developments in Radiative Heat Transfer*, American Society of Mechanical Engineers HTD-Vol. 203, 1992, pp. 119–127.

[7]Sparrow, E. M., and Cess, R. D., *Radiation Heat Transfer*, Hemisphere, New York, 1978.

[8]Ehlert, J. R., and Smith, T. F., "View Factors for Perpendicular and Parallel Rectangular Plates," *Journal of Thermophysics and Heat Transfer*, Vol. 7, No. 1, 1993, pp. 173–175.

[9]Fischer, W. D., private communication, The Aerospace Corp., Los Angeles, CA, 1992.

Measurement of the Absorption of Light by Polaroid Sheet

D. C. Look Jr.*
University of Missouri—Rolla, Rolla, Missouri 65401

Nomenclature

a = absorptance of the polarizer material
I = detector beam intensity (all polarizations)
I_H = detected horizontally polarized beam
I_v = detected vertically polarized beam intensity
I_0 = incident beam intensity
ε = relative alignment of an incident beam polarization and the axis of a polarizer

Introduction

VARIOUS publications involving the scatter of a linearly polarized laser beam at 90 deg by spherical particles in distilled water have been directed at presenting the resulting lobe-shaped scatter pattern.[1–4] When the incident laser beam is essentially circularly polarized, the detected variation in the scatter at 90 deg as a function of angle is very different.[5] An interesting offshoot of this study has been the development of a method to estimate the absorption of light by a linear polarizing sheet. This uncomplicated method is based on the general concepts of geometric optics.

Analysis

In an effort to describe the estimate, consider Fig. 1. This figure is the depiction of a linearly polarized beam of light of intensity I_0 incident upon a polarizer sheet. In traversing this sheet, the beam experiences two mechanisms that act to extinguish the beam. The first is the extinction of that portion of the beam whose polarization is not aligned with the axis of the polarizer sheet. The elimination of this component produces a linearly polarized beam whose axis is parallel to the axis of the polarizer. The second mechanism could be classified as standard absorption. This mechanism acts to eliminate a portion of the incident beam even if a linearly polarized incident beam is aligned with the polarizers. Without this second mechanism, a completely unpolarized incident beam I_0 would produce an output linearly polarized beam of intensity approximately $I_0/2$. That is, when the incident beam polarization and the polarizer axis are aligned, the beam passes through unscathed in terms of the polarized component being absorbed: there will be an absorption of the correctly aligned polarization component. A fraction a of the beam (aligned with the polarizer) will be absorbed. Thus the detected intensity in this case is

$$I = (1 - a)I_0 \tag{1}$$

A nonaligned beam and polarizer would require two measurements (one for each component), i.e.

$$I_v = (1 - a)I_0 \cos \varepsilon \tag{2}$$

$$I_H = (1 - a)I_0 \sin \varepsilon \tag{3}$$

Thus

$$\tan \varepsilon = I_H/I_v \tag{4}$$

$$a = 1 - [(I_v^2 + I_H^2)/I_0^2]^{1/2} \tag{5}$$

Table 1 Computed absorption coefficient of polaroid from linearly polarized incident light data of Ref. 5

Concentration, %	Detector depth, cm	Average particle size, μm				
		1.240	0.494	0.360	0.123	0.065
0.005	0.0	0.3168	0.3427	0.3137	0.3314	0.3500
	1.5	0.4273	0.3784	0.3248	0.2629	0.3035
	3.0	0.3609	0.3598	0.3249	0.2670	0.2849
0.0025	0.0	0.3274	0.3931	0.3007	0.2840	0.2884
	1.5	0.3216	0.2993	0.3014	0.2948	0.3191
	3.0	0.3410	0.3174	0.3018	0.2540	0.2587

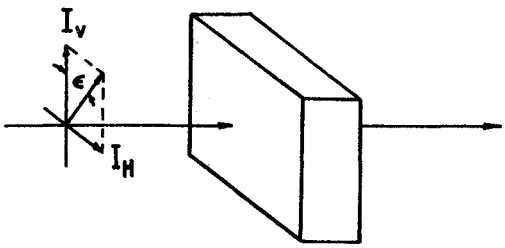

Fig. 1 Schematic of a nonaligned incident beam and polarizer.

Results

Equation (5) is particularly convenient as a basis for the computation of the absorption (the second mechanism) of the linearly polarizing element of an experiment considering the data reported in Ref. 5; total polarization I_0, horizontal polarization I_H, and vertical polarization I_v were measured. This absorption analyses was applied to all of the data reported in Ref. 5. The results are presented as Table 1. It may be noted that the polarization of the incident beam should not effect the absorption a; it does effect the angle ε. Thus, detector depth and particle size and concentration are not active parameters and do not effect the absorptance of the polarizing medium. The data in this table produce an average absorptance of $\bar{a} = 0.3184$. If a small sample statistic is used, the mean deviation and standard deviation are

$$\text{MD} = \frac{1}{n}\sum_{i=1}^{n} |a_i - \bar{a}| = 0.0286$$

$$\text{SD} = \left[\sum_{i=1}^{n} (a_i - \bar{a})^2/(n - 1)\right]^{1/2} = 0.0397$$

While these results are not ideal, they do represent the method and agree with the accepted absorptance of the standard HN 32 polaroid material of approximately 32% at a wavelength of 0.6328 μm (He Ne laser).[6]

Received Dec. 8, 1993; revision received Jan. 3, 1994; accepted for publication Jan. 3, 1994.

*Professor, Thermal Radiative Transfer Group, Mechanical and Aerospace Engineering and Engineering Mechanics Department. Associate Fellow AIAA.